A Lattice Model of Vitrification and Gelation

Jennifer E. Witman and Zhen-Gang Wang*

Division of Chemistry and Chemical Engineering, California Institute of Technology, Pasadena, California, 91125

Received: March 15, 2005; In Final Form: January 17, 2006

In this work we introduce a simple lattice model with T-shaped molecules in two dimensions that exhibits a rich range of morphological behaviors. Depending on the volume fraction and quench path, this system can adopt uniform liquid, solution, and phase-separated states, as well as inhomogeneous glass or gel-like states, as revealed by dynamic mean-field simulations. An important characteristic of this system is the existence of a large number of degenerate low-energy states with small barriers that leads to a broad, kinetically explored landscape. The mean-field stability and phase diagram of this model is constructed and provides a useful guide for understanding the complex behaviors of the system. One striking feature is that there is a cascade of instabilities that converge to mark the onset of what we identify as the glass transition. Both dynamic mean-field and Monte Carlo simulations reveal glass-like relaxation dynamics. Our results lead to a picture of gelation as a continuation of the glass transition into the two-phase region, or equivalently, as an incomplete phase separation arrested by the onset of the glass transition.

1. Introduction

There are natural parallels between the glass phase and physical gels (thermoreversible gels) as well as between vitrification and gelation. Recently, there has been considerable interest in unifying these two classes of disordered materials. For example, theory and simulation predict the existence of both glass- and gel-like structures in colloidal systems.[1−3] These predictions are consistent with features found experimentally.[4,5] In addition to structural similarity, dynamic observations have strengthened the conclusion that there is a relation between glasses and gels. Physical gels have associations with finite bond lifetimes (in contrast to chemically cross-linked gels). Experimental measurements of gelatin[6] and poly(vinyl alcohol) gels,[7] both thermoreversible polymeric gels, have shown glass-like relaxation dynamics. Colloids with short-range attractions share this property and can form gels at high densities that exhibit glass-like kinetic arrest[8,9] and relaxation properties.[10] In this work, we use a lattice model occupied by T-shaped molecules to explore the relation between glasses and physical gels.

The glass state has been studied in great detail, and the dynamics of many systems in addition to physical gels are analogous to those of a glass. Kauzmann, whose work was influential in the development of our current thermodynamic understanding of the glassy state, referred to the glass as one example of the "torpid" state,[11] a general category that includes linear polymers under flow and plastically deformed metals and crystals. Additionally, a variety of other materials demonstrate dynamic behavior characteristic of glass-like states. These include such diverse examples as the polycrystalline structure of thin films, protein folding,[12,13] and granular material jamming.[14]

Lattice models have been extensively used to explore both the structure and dynamics of the glassy state. Among the many examples, it is useful to contrast two classes. The first consists of models whose Hamiltonians directly induce frustration. By construction, these models do not have fully satisfied alignment states. There are no configurations that satisfy all of the locally preferred low-energy states. Ising spin glasses,[15] in which the interactions are randomly assigned to favor parallel or antiparallel orientation, are classical examples. Conversely, there are models whose rules of motion make the formation of macroscopic uniform phases unlikely. Falling under the umbrella of hierarchically constrained local dynamics, the evolution in time of these Ising-type models is restricted by the state of neighboring sites.[16] These include the Fredrickson−Anderson-facilitated kinetic Ising models[17] and the East model.[18] In a similar manner, the tiling model[19] and a recent model by Garrahan and Chandler[20] demonstrate glassy dynamics based on local dynamical rules, although the coarse-graining implicitly does not include the crystal state. Our model does not exclude ordered states; however, unlike traditional liquids, these states have the same energy as that found in satisfied yet inhomogeneous states.

One way to capture the features and behavior of amorphous solids on a lattice is to assign anisotropic interactions. Aranovich and Donohue explored the role of anisotropy on molecular fluids.[21] Highlighting that most molecules and particles have anisotropic interactions due to the steric limitations of arrangement and bonding constraints, they considered a variety of phase transitions, including condensation, crystallization, and polymerization. Developed concurrently are several other models of Ising-like lattice liquids and glasses that in some way restrict the number of nearest neighbors on the lattice, leading to glassy features.[22,23] In a similar manner, Del Gado et al. employed a model in which monomers occupy a cubic lattice and are tetrafunctional, allowing for vacant sites within the network without energetic penalty.[10] The presence of telechelic monomers that can form a network with "solvent" intuitively leads to a picture of a polymeric gel.

A minimal requirement for network formation in two dimensions is a trimer structure that allows junctions and branching. The Mercedes-Benz model[24,25] (named for its resemblance to the famous logo) has three directional arms, each capable of

* Corresponding author. E-mail: zgw@cheme.caltech.edu.

10.1021/jp051365e CCC: $33.50
Published on Web 03/04/2006

supporting hydrogen bonding. There is an energetic balance between the advantageous formation of an open "bonded" structure, in which the arms of the monomers touch, and a force favoring an incommensurate dense structure. This model has been studied in both on-lattice[25] and off-lattice[24,26] formulations. Other on-lattice[27] and off-lattice models of water[28] distinguish between hydrogen bonds and van der Waals forces determined by the relative orientation of the monomers. Our model features anisotropic interactions that lead to the number of bonds formed being smaller than the number of nearest neighbors. In addition to sharing this feature with geometrically constrained systems (e.g., colloidal particles with short-range interactions), our model is naturally relevant to network-forming liquids such as silica glasses[29] and water,[30,31] in which the interactions are due to directional bonds.

Gelation has commonly been associated with geometrical percolation. However, this condition is not sufficient to describe the transition in physically associating gels. These systems, which have bond lifetimes comparable to or shorter than the time scale of interest in experiments, may not exhibit solid-like character at the geometric percolation threshold.[32,33] Further, simulations by Kumar and Panagiotopoulos show no change in a thermodynamic property at gelation, suggesting that gelation is not a higher-order thermodynamic transition.[34] The specific molecular interactions yield rich behavior in some physical gels that does not conform to the percolation model.[35]

We endeavor to link the glass transition and gelation within a lattice model that can encompass both glass and physical gel phases in appropriate relation to the liquid and solution phases. We investigate the properties of a lattice occupied by T-shaped molecules whose anisotropic nature leads to a wide variety of morphological states. We explore these states by using a dynamic mean-field (DMF) simulation method that, by construction, evolves toward a free-energy minimum as well as a Monte Carlo (MC) method. Glassy or gel-like behaviors are identified as corresponding to free-energy minima associated with inhomogeneous and nonperiodic structures.[36]

Our primary concern in this work is to understand the thermodynamic and kinetic factors leading to such amorphous structures. We have also completed initial work investigating the dynamics of our model system. We propose that these amorphous, glass or gel-like structures arise as a result of the proliferation of a large number of such inhomogeneous free-energy minima, which is intimately connected to an underlying spinodal of the uniform liquid or solution phase with respect to inhomogeneous fluctuations. However, the resultant structures depend on the "processing" or quenching conditions. Therefore their origin is both thermodynamic and kinetic in nature. Our study suggests that a mechanism for gelation is incomplete phase separation in the two-phase region of the phase diagram arrested by the onset of glass transition.

2. T-Shaped Molecule Model

We consider a two-dimensional square lattice of $N \times N$ sites. Each lattice site is either occupied by a three-armed, T-shaped molecule or is vacant, representing a solvent molecule. The T-shaped molecule can take any of the four orientations designated as 1, 2, 3, and 4 in Figure 1a. The vacant state (not shown) is denoted as state 5. Each arm of the T-shaped molecule is capable of forming an association (bond) of energy $-\epsilon$ with the adjoining arm from a nearest neighbor molecule. The added level of complexity in our model arises from both the state of a site (vacant or occupied with orientation 1, 2, 3, or 4) and the relative orientation of the molecule at that site with respect to its neighboring sites. This relative orientation determines the association state, as the molecule is anisotropic.

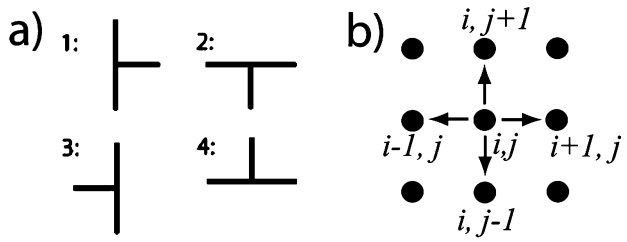

Figure 1. (a) States of the T-shaped molecules on a square lattice. The model contains these four states and a fifth state (not shown) that represents a vacancy. (b) The relative orientation between site i,j and its nearest neighbors.

We will denote the occupancy of a site (i,j) in state a by $\hat{p}_a(i,j)$ [$\hat{p}_a(i,j) = 1$ if site (i,j) is in state a, and 0 otherwise; and $\sum_{a=1}^{5} \hat{p}_a(i,j) = 1$]. The Hamiltonian of our system is written as

$$\begin{aligned}\beta H = -\left(\frac{\beta\epsilon}{2}\right)\sum_{i=1}^{N}\sum_{j=1}^{N}\{&\hat{p}_1(i,j)[\hat{p}_1(i,j+1) + \hat{p}_2(i,j+1) + \\ &\hat{p}_3(i,j+1) + \hat{p}_2(i+1,j) + \hat{p}_3(i+1,j) + \hat{p}_4(i+1,j) + \\ &\hat{p}_1(i,j-1) + \hat{p}_3(i,j-1) + \hat{p}_4(i,j-1)] + \hat{p}_2(i,j)[\hat{p}_2(i+1,j) + \\ &\hat{p}_3(i+1,j) + \hat{p}_4(i+1,j) + \hat{p}_1(i,j-1) + \hat{p}_3(i,j-1) + \\ &\hat{p}_4(i,j-1) + \hat{p}_1(i-1,j) + \hat{p}_2(i-1,j) + \hat{p}_4(i-1,j)] + \\ &\hat{p}_3(i,j)[\hat{p}_1(i,j+1) + \hat{p}_2(i,j+1) + \hat{p}_3(i,j+1) + \hat{p}_1(i,j-1) + \\ &\hat{p}_3(i,j-1) + \hat{p}_4(i,j-1) + \hat{p}_1(i-1,j) + \hat{p}_2(i-1,j) + \\ &\hat{p}_4(i-1,j)] + \hat{p}_4(i,j)[\hat{p}_1(i,j+1) + \hat{p}_2(i,j+1) + \hat{p}_3(i,j+1) + \\ &\hat{p}_2(i+1,j) + \hat{p}_3(i+1,j) + \hat{p}_4(i+1,j) + \hat{p}_1(i-1,j) + \\ &\hat{p}_2(i-1,j) + \hat{p}_4(i-1,j)]\} - \left(\frac{\beta\eta}{2}\right)\sum_{i=1}^{N}\sum_{j=1}^{N}\hat{p}_5(i,j)[\hat{p}_5(i,j+1) + \\ &\hat{p}_5(i+1,j) + \hat{p}_5(i,j-1) + \hat{p}_5(i-1,j)] \quad (1)\end{aligned}$$

For completeness, we have included an isotropic interaction between the solvent molecules (or, equivalently, between the solute molecules by virtue of the occupancy constraint). In this work, we consider the case $\eta = 0$.

We have employed the following dynamic rules of motion for our model. The molecules can undergo both rotational and translational diffusion. During rotation, a T-shaped molecule can interchange states 1, 2, 3, or 4 at a given site. We do not attempt to mimic the actual physical rotation of the T-shaped molecules and will thus allow a T-shaped molecule to rotate from a given state to any of the other states in a single time-step. For translational diffusion, we use Kawasaki-exchange dynamics[37] between a T-shaped molecule and a nearest neighbor solvent molecule as well as for the self-diffusion, or exchange, of neighboring T-shaped molecules. In the fully dense region of our phase diagram, there is no fundamental difference between rotational and translational diffusion.

In this work we employ both the Metropolis MC simulation technique[38] as well as the DMF simulation method.[39] Thus far, MC simulations have only been performed on a fully dense lattice with no vacancies. The MC simulations proceed by selecting a site at random and then proposing a change in its orientation or an exchange with a nearest neighbor; this rule would be equally applicable where there are vacancies. The Metropolis recipe is used to determine whether this change is accepted.

The DMF simulations (to be discussed further in section 3) can be considered a mean-field implementation of MC dynam-

ics.[39] However, for computational purposes, it is convenient to use the Barker form[40] of the transition probability, $q_{\text{current}\to\text{new}}$:

$$q_{\text{current}\to\text{new}} = \omega \frac{\exp(-\beta E_{\text{new}})}{\exp(-\beta E_{\text{current}}) + \exp(-\beta E_{\text{new}})} \quad (2)$$

instead of the Metropolis form ($q_{\text{current}\to\text{new}} = \omega$ if $E_{\text{new}} < E_{\text{current}}$, and $q_{\text{current}\to\text{new}} = \omega \exp[-\beta(E_{\text{new}} - E_{\text{current}})]$ if $E_{\text{new}} > E_{\text{current}}$). In eq 2, ω is an attempt frequency (which can be different for the rotational and translation moves), and E_{current} and E_{new} are respectively the energy of the system in its current state and new state. As in the MC simulations, the new state reflects both orientation change and nearest neighbor exchange. The dynamics in the DMF evolution of the singlet density at each lattice site follow a steepest descent path into a free-energy minimum.

2.1. Role of Anisotropic Interactions. The anisotropy of the model, which allows for orientational disorder and mimics bonding and steric constraints, plays a strong role in the type of quenched structures we observe. The organizing feature of this model is the presence of a nonbonding side or "back". Before exploring the phase diagram in detail, it is helpful to consider some of the phases the lattice can adopt. In our DMF simulations (to be described later in section 3) we can identify whether a particular site was strongly oriented and would persist in that state over time. These sites are shown in black in the figures. Sites that are not strongly oriented appear in gray. Sites that are most probably solvent molecules are represented as blanks.

In the fully dense limit, without solvent, the molecules must be arranged in pairs back to back in order for the lattice to be satisfied. Otherwise, there is an associating end presented to a nonbonding side. These satisfied structures can be crystal-like (Figure 3a) or amorphous (Figure 3b), depending on the pattern of the pairs. The amorphous structures can also contain unsatisfied sites at which not all arms form bonds with their neighbors. These sites are still liquid-like in that they retain equal probability to arrange in any orientation.

In other regions of the phase diagram, the back of the molecule points toward the solvent. This gives the molecule a self-surfactant character. The molecules can be arranged in phase-separated, highly satisfied states (Figure 7) or in gel-like states (Figures 8 and 10). In observing gel-like structures, two features are clear. The first is that the structures involve at least a pair of molecules that form ladder-like structures. The second is that there are unsatisfied sites located at the junctions of the fibrils. Gel-like features are observed under a wide range of conditions. The particular characteristics of the gel-like state, for example, the fibril length and width, can be varied by altering the simulation conditions.

3. DMF Simulations

The DMF simulation technique is a deterministic method for evolving the singlet mean-field probability, p_a, of the lattice sites from a given initial condition.[39] It is similar to the dynamic density functional methods for molecular[41] and polymeric fluids.[42] Given the dynamic rules for a lattice model, the DMF equations of motion are obtained from a local mean-field approximation of the master equation corresponding to those rules. The DMF simulation method has formulations for both conserved and nonconserved order parameters. The governing equations and detailed balance conditions for both cases were derived in the reference.[39] Below, we present the application of these equations to our current model.

3.1. DMF Equations. The probability that a lattice site (i,j) will be in state a at time t is given by $p_a(t;i,j)$. Our master equation encompasses both rotational diffusion and translational diffusion. The overall probability that a molecule will be found in a particular orientation (states 1, 2, 3, and 4) on the lattice is not conserved. However, the number of molecules on the lattice remains constant, requiring conserved motion. These two forms of motion are captured in the master equation under the mean-field approximation given by

$$p_a(t+1;\vec{i}) = p_a(t;\vec{i}) + \sum_{b\neq a}[q(t;i;b\to a)p_b(t;\vec{i}) - q(t;i;a\to b)p_a(t;\vec{i})] + \sum_{\langle \vec{i}',\vec{i}\rangle}\sum_{c\neq a}[q(t;c,\vec{i}'\leftrightarrow a,\vec{i})p_c(t;\vec{i}')p_a(t;\vec{i}) - q(t;a,\vec{i}'\leftrightarrow\gamma,\vec{i})p_a(t;\vec{i}')p_c(t;\vec{i})] \quad (3)$$

for the first four states ($a = 1-4$), and

$$p_5(t+1;\vec{i}) = p_5(t;\vec{i}) + \sum_{\langle \vec{i}',\vec{i}\rangle}\sum_{c\neq 5}[q(t;c,\vec{i}'\leftrightarrow 5,\vec{i})p_c(t;\vec{i}')p_5(t;\vec{i}) - q(t;5,\vec{i}'\leftrightarrow c,\vec{i})p_5(t;\vec{i}')p_c(t;\vec{i})] \quad (4)$$

for the solvent. The summation in eq 3 over b includes states 1−4, and the summation in both equations over c includes all states. We use the vector $\vec{i}$ to denote the two-dimensional coordinates, and $\langle\vec{i}',\vec{i}\rangle$ indicates that $\vec{i}$ and $\vec{i}'$ are nearest neighbor sites. The term $q(t;i;b\to a)$ is the transition probability for rotation from state b to state a. The transition probability for translation, $q(t;c,\vec{i}'\leftrightarrow a,\vec{i})$, involves exchanging the states between site $\vec{i}$ and its nearest neighbor $\vec{i}'$. Consistent with the mean-field approximation at the singlet density level, these transition probabilities can be written simply as[39]

$$q(t;i;a\to b) = \omega_1 \frac{\exp[-\beta E_b(t;\vec{i})]}{\exp[-\beta E_a(t;\vec{i})] + \exp[-\beta E_b(t;\vec{i})]} \quad (5)$$

and

$$q(t;a,\vec{i}\leftrightarrow b,\vec{i}') = \omega_2 \frac{\exp[-\beta(E_a(t;\vec{i}') + E_b(t;\vec{i}))]}{\exp[-\beta(E_a(t;\vec{i}) + E_b(t;\vec{i}'))] + \exp[-\beta(E_a(t;\vec{i}') + E_b(t;\vec{i}))]} \quad (6)$$

In our calculation, we take ω_1 to be 1/6 and ω_2 to be 1/24. Also, the temperature of our system is always taken to be that of the final condition resulting in "instantaneous" quenches. The energy appearing in the transition probabilities is given by $E_a(t;i) = \partial H/\partial p_a(t;i)$, where H is the mean-field energy of the system (eq 1), with the fluctuating $\hat{p}_a(t;\vec{i})$ replaced by the average $p_a(t;\vec{i})$. As an example,

$$E_1(t;i,j) = \frac{\partial H}{\partial p_1(t;i,j)} = \frac{-\epsilon}{2}[p_1(t;i,j+1) + p_2(t;i,j+1) + p_3(t;i,j+1) + p_1(t;i,j-1) + p_3(t;i,j-1) + p_4(t;i,j-1) + p_2(t;i+1,j) + p_3(t;i+1,j) + p_4(t;i+1,j)] \quad (7)$$

where we reintroduce the two-dimensional lattice coordinates to emphasize the relative orientation of the T-shaped molecules with respect to the direction of its nearest neighbors.

The master equation will evolve with time until it reaches a stationary state. This stationary state is a result of detailed balance which is given by

$$p_a(\vec{i})q(i;a\rightarrow b) = p_b(\vec{i})q(i;b\rightarrow a) \quad (8)$$

and

$$q(c,\vec{i}\,'\leftrightarrow a,\vec{i})p_c(\vec{i}\,')p_a(\vec{i}) = q(a,\vec{i}\,'\leftrightarrow c,i)p_a(\vec{i}\,')p_c(\vec{i}) \quad (9)$$

By virtue of the choice of the transition probabilities that satisfy detailed balance, the DMF equations will evolve the system toward an equilibrium or metastable equilibrium state. Thus, the stationary solutions of the DMF equations correspond to free-energy minima. Glassy or gel-like phases are identified as inhomogeneous, nonperiodic, stationary solutions of the DMF equations. Although the DMF equations cease to evolve at these stationary solutions, and would hence lead to complete structural arrest, such a result is a manifestation of the deterministic nature of the mean-field equations. In the presence of random thermal motion, the system would continue to evolve through activated processes by jumping out of the local free-energy minima. Nevertheless, the *existence* of such free-energy minima indicates structural arrest on some short time scales and hence signals a change in the character of the dynamics of the system. Therefore, in addition to describing the temporal evolution of the system at the mean-field level, the DMF simulation technique provides a useful method for searching and locating these inhomogeneous free-energy minima.

4. Fully Dense System: Liquid, Crystal, and Glass Phases

In this section, we consider the behavior of the fully dense system (where there is no solvent or state 5) under the mean-field approximation. We start with an overview of the phase behavior in this region before proceeding to calculate the transition temperature between the liquid and the vitrified phases as well as the spinodal of the liquid phase. With this analysis as a guide, we then use DMF simulations to characterize the response of the liquid to fluctuations and investigate the morphology of the solid.

4.1. Overview of Phase Behavior. In the fully dense region ($p_5 = 0$), the lattice can assume a liquid phase or a solid configuration. At high temperatures, there is an equal probability that the molecules will be found in any of the four states ($p_1 = p_2 = p_3 = p_4 = 1/4$); we identify this state with the liquid phase. At sufficiently low temperatures, the T-shaped molecules at most of the lattice sites become strongly oriented in one of the four orientations. A simple mean-field calculation predicts a first-order transition from the liquid state to these locally oriented solid states. Mean-field theory also predicts a spinodal for the liquid state below which a metastable liquid can no longer exist. As this spinodal signals the spontaneous appearance of inhomogeneous free-energy minima, we associate it with the ideal glass transition of this model. The crystalline state in this model—an alternating bilayer structure—is a peculiar state. Unlike many physical glasses, the crystalline state in our model has no energetic advantage over other amorphous configurations. Its appearance is a result of a particular kinetic path. For our purpose, the existence of this crystalline state has no special significance. There are a vast number of equivalent lowest-energy states that have all the arms bonded or satisfied (more details will be given in section 6.1).

4.2. Transition between the Liquid and the Vitrified States. Instantaneously quenched from the high-temperature liquid to the low-temperature crystalline or glassy states, the T-shaped molecule at an individual lattice site transitions from having an equal probability of being oriented in any of the four states to strongly preferring one state. Characterization of the glass-like configurations requires specifying the spatial probability distribution of the molecule orientation of the full lattice. As this is analytically intractable, we make a simplifying approximation that each site is dominated by one particular orientation, and all the other orientations have equal probabilities. Furthermore, we assume that the probability of the dominant orientation is the same for all lattice sites (although the dominant orientations at different lattice positions need not be the same). While the validity of these assumptions is not immediately obvious, our DMF simulation confirms that the vast majority of sites have the same bias toward a dominant local orientation and that the subdominant orientations have approximately equal probabilities.

Taking the dominant probability to be p_1, we can write an approximate free energy per site for the solid state as

$$\beta f_{\text{solid}} = -(1/2)\beta\epsilon(3{p_1}^2 + 12p_1p_2 + 21{p_2}^2) + p_1 \ln p_1 + 3p_2 \ln p_2 \quad (10)$$

where we have made use of our assumption that $p_2 = p_3 = p_4$. In this calculation, we do not distinguish between the crystal-like and the glass-like solid states because we neglect the details of the structure on the lattice. Therefore, this free energy also describes the bilayer crystalline structure described in section 4.5.[43]

The equilibrium state is obtained by minimizing the free energy with respect to these probabilities. Phase transition occurs when this free energy equals that of the liquid with unbiased orientation distribution:

$$\beta f_{\text{liq}} = -(9/8)\beta\epsilon - \ln 4 \quad (11)$$

We find a first-order transition at $\beta\epsilon = 3 \ln 3$, with the solid-state having $p_1 = 3/4$, $p_2 = p_3 = p_4 = 1/12$ at the transition.

4.3. Stability Limit of the Uniform Liquid Phase. Because the transition from the uniform liquid to the solid phase is first order, the formation of the solid phase from a metastable liquid involves a nucleation barrier. It is therefore possible to supercool the liquid below the freezing temperature. However, this supercooling can only proceed as far as the spinodal, or metastability limit of the liquid. Beyond this limit, the uniform liquid becomes unstable with respect to an infinitesimal inhomogeneity in the probability distributions; that is, an inhomogeneous structure will form spontaneously. Each of these inhomogeneous (amorphous) structures corresponds to a local free-energy minima. Since, in the mean-field picture, there are no activated events, a system, having reached one such free-energy minimum, is permanently trapped there. This consideration motivates us to identify the spinodal as the mean-field signature for an "ideal" glass transition. In this sense, the spinodal temperatures can be likened to the Kauzmann temperature T_k, the lowest temperature for the onset of the glass transition. We note that other authors have previously hinted at the connection between the liquid spinodal and an ideal glass transition.[44−46] This conclusion has been explicitly demonstrated in the case of block copolymer microstructural glasses.[47] In reality, because of thermal fluctuation, the system can fall into these amorphous states earlier than the spinodal, as well as escape them and diffuse between minima.[31]

The spinodal of the liquid can be easily obtained by examining the second derivative of the free-energy expression, eq 10. Setting this derivative to zero, we find that the spinodal occurs at $\beta\epsilon = 4$. This value agrees with a more systematic calculation by finding the lowest eigenvalue of the second derivative matrix of the full mean-field free-energy function as calculated in section 5.3.

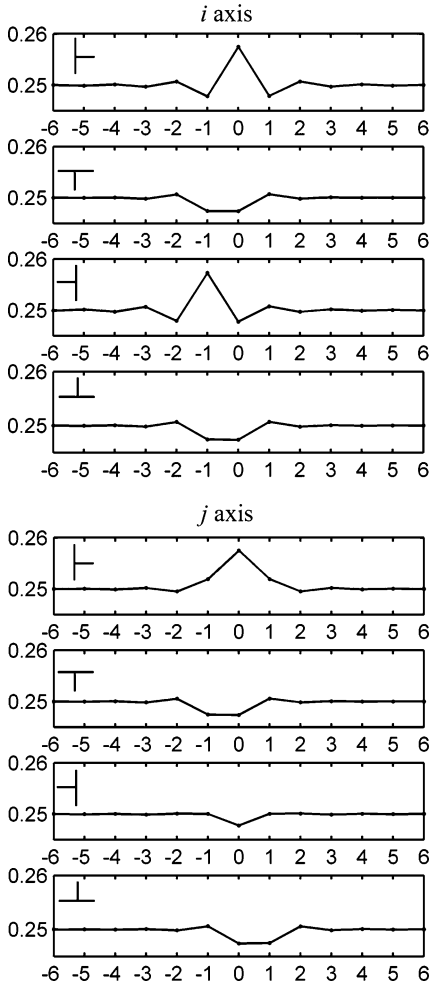

Figure 2. The probability of being in each state as a function of position along the *i* and *j* axes, after a small pinning force of magnitude 0.0001β favoring state 1 is applied at site (0,0) to a fully dense lattice. The unperturbed liquid-like state at $\beta\epsilon = 3.92$, $\rho = 1$ has an equal probability (0.25) of being in each state.

4.4. Correlation in the Liquid State. With the theoretical analysis of the mean-field behavior as a guide, we now proceed to examine the system in the fully dense phase using the DMF simulation. While the equilibrium probability of a site being in each of the four orientations is equal in the liquid state, the anisotropy of the interactions leads to nontrivial spatial correlations. Within mean-field theory, these correlations can be examined by the response of the system to a small localized perturbing field. Figure 2 shows the probability profile for the four different states on the *i* and *j* axes when site (0,0) is perturbed by a field of magnitude 0.0001β that favors state 1. The system is a liquid at $\beta\epsilon = 3.92$, $\rho = 1.0$.

Because the field at the origin (0,0) favors state *1*, the probability of this state at site (0,0) is enhanced at the expense of the other three states. More reflective of the anisotropy of the interaction are the probability of the states next to (0,0). For example, state 1 is depleted both to the left and to the right, whereas states 2, 3, and 4 are enriched to the right. The site (−1,0) is particularly interesting since state 3 is enriched while all other states are suppressed. These trends, as well as the special symmetry of the profiles along the *j* axis, can all be rationalized by the energetic preference to have the arms of the molecules pointing to each other and not to have the arm of a molecular facing the back of another.

The effects of the field at site (0,0) diminish as we move far from the origin, manifesting as a damped small oscillation with respect to the bulk value. A correlation length can be defined as the length scale for the decay of the probability profiles to their bulk value; the correlation length shows the characteristic square-root divergence with the proximity to the spinodal as expected from the mean-field behavior. However, the numerical prefactor turns out to be unusually small, the correlation length reaching only a few lattice spacings when *T* is within 1% of the spinodal.

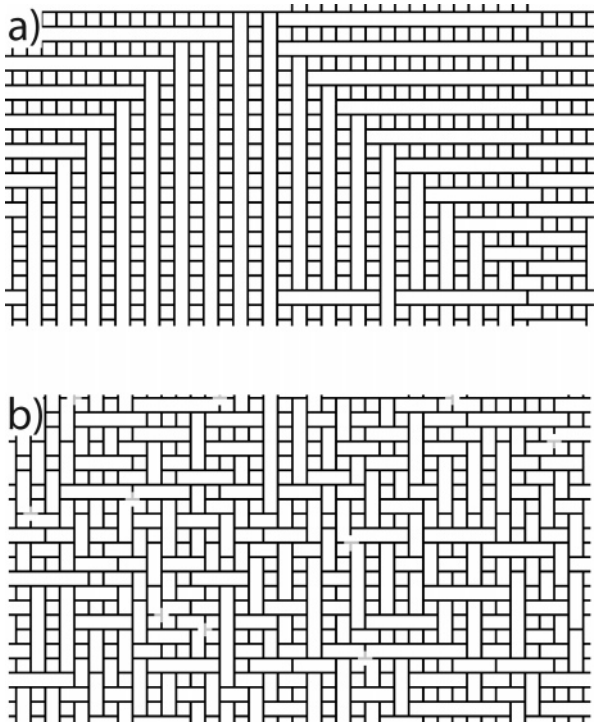

Figure 3. DMF simulation results: (a) crystalline state ($\beta\epsilon = 3.7$, ρ=1) and (b) glassy state ($\beta\epsilon = 4$, ρ=1). Both simulations were started from a liquid state with small perturbations before instantaneously quenching to the final conditions. The black molecules are strongly oriented in the indicated direction. The gray molecules indicate that the site has equal probability of being in any of the four orientations. The orientation at these sites is chosen randomly in the figure.

4.5. Vitrification in DMF Simulations. We can investigate the morphology of the solid-like state using DMF simulations. Starting with the isotropic liquid state at high temperature where the four orientations are equal on all lattice sites, we quench the system instantaneously to a lower temperature. Since the DMF equations are deterministic, we add small random perturbations in the probabilities to provide the initial driving force for setting the equations into motion. Above the liquid−solid transition temperature, we find that the lattice of probabilities relaxes back to the isotropic liquid state. For sufficiently small perturbations, it is possible to supercool the liquid below the transition temperature. However, at some temperature between the transition and spinodal temperatures, a sufficiently large local perturbation will be able to overcome the nucleation barrier and induce growth of the solid phase. Figure 3a shows a typical configuration of the crystalline state obtained from a shallow quench past the coexistence temperature. In this configuration, all the molecules on the lattice are satisfied; each associating end group is paired.

The formation of a crystal-like phase when a small number of nucleation sites exists is a kinetic phenomena, not a thermodynamic one. Fully bonded amorphous states share the same entropy and energy. The tendency to form a crystalline region arises from the propensity to bury the "back" or nonbonding side of the molecule. Figure 4 shows the evolution

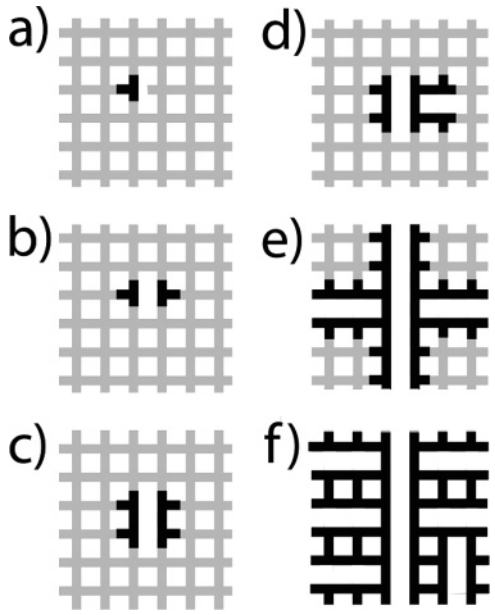

Figure 4. Progression of the DMF simulations from a nucleation point. The oriented (solid-like) T-shaped molecules are shown in black, while the gray T-shaped molecules represent those that are not oriented (are liquid-like).

of a crystalline state in frames a−f. As described in section 4.4, the response of a liquid to a fluctuation is anisotropic; this has a strong influence on the kinetics of orientation surrounding a nucleation site. Consider for a moment one nucleation event, for example, the molecule at lattice site (i,j) oriented in state 3, with a probability that upsets the metastability of the system (Figure 4a). The initial bias will tend to orient its neighbor to the right in the opposite direction, state 1 (Figure 4b), as this orientation presents the largest probability for all the arms of the neighboring sites to be bonded.

The surrounding sites of this initial pair experience an environment that has strong orienting properties. The pair above the nucleus now will experience a strong tendency to align one of their associating ends with the associating ends pointing downward from the initial sites. To best take advantage of the energetics, the new pair will align in the same direction as the previous pair. This initiates the formation of a lamella (Figure 4c).

From the sides of this initial lamella will evolve lamella oriented in the orthogonal direction (Figure 4d). Again, the organizing feature is the anisotropic nonbonding side. As the growth occurs in an outward manner, eventually the different domains of lamella begin to influence the growth of each other (Figure 4e). At the intersection, there are a variety of satisfied orientations that can be adopted (Figure 4f).

When the system is instantaneously quenched to a temperature past the spinodal, spatial inhomogeneities in the probability distribution grow spontaneously. Unlike the isolated nucleation events that occur between the coexistence temperature and the spinodal, the simultaneous growth of all instabilities leads to heterogeneous microenvironments. The thermodynamic driving force for the T-shaped molecules to form associating bonds with their neighbors becomes sufficiently strong, such that most or all adopt a preferred orientation. The T-shaped molecules attempt to maximize the number of bonds by choosing the locally optimal orientation determined by their microenvironments. The orderly growth of crystal-like structures at higher temperatures is replaced by the simultaneous formation and growth of bonded clusters, which eventually grow to a large network. The resulting structure appears very amorphous, without clear crystalline ordering. In this structure, most sites are satisfied; that is, their three arms are held strongly by bonds formed with their neighbors. However, because the structure results from the uncoordinated formation of associating bonds driven by the local needs of the molecules, some molecules may be left unsatisfied. These sites are shown in gray in Figure 3b. While one orientation is chosen randomly at each of these sites for the purpose of illustration, these gray sites retain their liquid character ($p_1 = p_2 = p_3 = p_4$).

5. Solvated Phases: Gel-like Structures with Glassy Features

In this section we explore the variety of morphologies that are observed when solvent (state 5) is present. We start with a discussion of the role that the solvent plays in the system and an investigation of the high-temperature solution state. We follow this by a calculation of the mean-field phase diagram and our analysis of the spinodals. Finally, we present simulation results that highlight the role of the glass transition in arresting phase separation.

5.1. Role of Solvent in Phase Behavior. When solvent is present, the interplay between phase separation and vitrification generates a variety of morphologies, including uniform solutions, phase-separated droplets, and a range of gel-like structures such as foamlike, networked, and fibril-like morphologies. Which of these structures is observed in the simulation depends closely on the quench conditions.

We observe the solution phase above the coexistence line. The solvent and the T-shaped molecules are equally distributed over the lattice. The solute has an equal probability of being in any of the four states ($p_a(i,j) = \rho/4$ for $a = 1$, 2, 3, and 4, and $p_5(i,j) = 1 - \rho$). At lower temperatures, the lattice will phase-separate into solvent-rich and solute-rich phases. The solute-rich phase can either be an isotropic liquid phase or be in a glassy state, depending on the concentration and temperature.

The interface between solvent- and solute-rich phases plays an important role in the local, morphological organization. The solute prefers to orient in such a way that its nonbonding side is adjacent to the solvent. This orients the molecule so that the associating groups are pointing toward the denser, solute-rich region, regardless of whether this region is still solution-like or has adopted a glassy configuration. The anisotropic nature of the T-shaped molecule causes it to behave as a surfactant at the interface between the T-shaped molecule-rich phase and the solvent.

5.2. Mean-Field Phase Diagram. We calculate the equilibrium phase diagram using the simplest approximation involving the singlet density. Although higher-order approximations can be constructed without too much difficulty, we choose this level of approximation so as to be consistent with the level of mean-field approximation in the DMF simulation.

In the absence of orientational order, the liquid−liquid coexistence curve can be easily obtained. Assuming equal probability of the solute being oriented in each of the four orientations ($p_1 = p_2 = p_3 = p_4 = \rho/4$), the free energy per site is simply

$$\beta f = -(9/8)\beta\epsilon\rho^2 + \rho \ln(\rho/4) + (1 - \rho) \ln(1 - \rho) \quad (12)$$

This is similar to the Bragg−Williams free energy for a lattice gas,[48] with the factor of 1/4 inside the logarithm having no effect on the phase diagram.[49] Equation 12 predicts a symmetric phase diagram with a critical point at $\beta\epsilon = 16/9$.

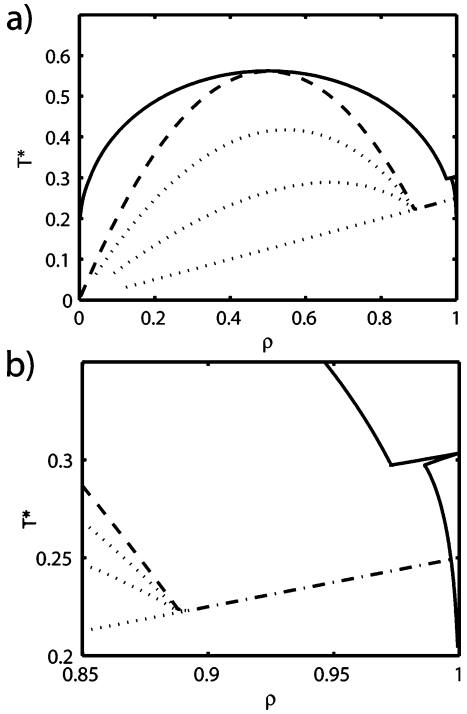

Figure 5. (a) Phase diagram: binodal (solid line), macroscopic spinodal (dashed line) local ordering spinodal (dot−dashed line), and cascade of spinodals within the liquid−liquid spinodal (dotted lines). $T^* \equiv (\beta\epsilon)^{-1}$ is the dimensionless temperature. (b) An expanded view of the high solute density region around the transition temperature for the glass-like phase.

For sufficiently low temperatures, we expect the high-density phase to be the vitrified phase with locally broken orientation symmetry. Since the free energy of the lamellar crystalline state is identical to that of the glassy state in our approximate treatment of the glassy phase in the fully dense state, we will not distinguish between these two states here either. For the purpose of constructing the phase diagram, we will characterize the glassy phase the same way we characterize the fully dense case ($p_1 > p_2 = p_3 = p_4$). This characterization amounts to a uniform dilution approximation, in which the effect of the solvent is simply to change the normalization of the probabilities from $\sum_{a=1}^{4} p_a = 1$ to $\sum_{a=1}^{4} p_a = \rho$. Under this approximation, the free energy of the glass-like state becomes

$$\beta f_{\text{ran}} = -(1/2)\beta\epsilon[3{p_1}^2 + 4p_1(\rho - p_1) + (7/3)(\rho - p_1)^2] + p_1 \ln p_1 + (\rho - p_1)\ln[(\rho - p_1)/3] + (1 - \rho)\ln(1 - \rho) \quad (13)$$

where the last term accounts for the entropy due to the presence of solvent.

Using eq 13, the probability of the dominant orientation is obtained by minimizing the free energy with respect to p_1. The coexistence between the glassy state and the isotropic liquid or gas phases is calculated by equating the chemical potential ($\beta\mu = (\partial\beta f/\partial\rho)$) and the grand potential density ($\beta w = \beta f - \beta\mu\rho$). The phase diagram is shown in Figure 5 with a triple point at $\beta\epsilon \approx 3.37$, $\rho \approx 0.97$.

5.3. Analysis of the Spinodals. As in the fully dense case, the spinodal plays an important role in determining the thermodynamic and kinetic behavior of the system when solvent is present. With the DMF equations of motion, it is possible to perform a linear stability analysis of the uniform state and determine the linear rate of growth of the unstable modes that are consistent with the dynamic rules of the model. For simplicity, however, here we will examine the issue of stability based purely on a consideration of the free energy. The spinodal or limit of metastability is determined by evaluating the matrix of the second derivatives of the free energy:

$$F^{(2)}[a,i,j;a',i',j'] = \frac{\partial^2 F}{\partial p_a(i,j)\partial p_{a'}(i',j')} \quad (14)$$

where F is the Helmholtz free energy as a function of the spatially varying singlet probabilities. We construct the matrix explicitly on a 16×16 lattice and diagonalize the matrix to find its eigenvalues. The vanishing of the lowest eigenvalue defines the spinodal. The result is shown in Figure 5.

Inside the liquid−liquid coexistence, we have the usual spinodal of the uniform liquid with respect to macroscopic phase separation (dashed line). In the high density region, there is another spinodal that corresponds to the limit of stability of the uniform liquid with respect to spatially inhomogeneous probability distribution on length scales of the size of the lattice spacing (dot−dashed line). This spinodal is the extension of the one occurring at $\beta\epsilon = 4$ in the fully dense state. As we decrease the temperature inside the envelope of the macroscopic spinodal, additional instabilities set in that represent progressively smaller length scales (dotted lines). We represent the onset of these new unstable modes by a family of curves as they move down the temperature. We note that, while both the liquid−liquid coexistence curve and the macroscopic spinodal curve are symmetric, these higher modes of instability become skewed toward high density, presumably reflecting the tendency for orientational ordering. The most striking feature of this cascade of instabilities is that they converge to an extension of the spinodal of the uniform liquid with respect to local orientational ordering as temperature decreases. These higher instabilities will be crucial for determining the morphology of quenched structures in the two-phase region. We note that the phase behavior implied by our phase diagram is very similar to the general phase diagram of a physical gel, lending confidence to our assertion of gel-like features.[50]

5.4. Correlations in the Solution Phase. As in section 4.4, we measure the correlation in the system via the introduction of a small biasing field to a single site. Because of the anisotropy of the system, the resultant probability profile is again different for each state. In Figure 6, we show the profiles for each state along the *i* and *j* axes for a solution at $\beta\epsilon = 1.7$ near the critical point of $\beta\epsilon = 16/9$. For these calculations, we use the grand canonical ensemble and set the chemical potential so that the unperturbed solution is kept at a density of $\rho_c = 0.5$ solute. We bias the probability of state 1 to be higher at site (0,0) by introducing a field of magnitude 0.01β at that site.

Overall, there is an increase in solute density near the site of the perturbation. However, the self-surfactant characteristic of the molecule results in a very different probability profile when solvent is present compared to the fully dense liquid. In the negative *i* direction, the perturbation has almost no effect on the probability profile, whereas the profiles are remarkably symmetric along the *j* axis. This significant asymmetry between the positive and negative *i* directions as well as between the *i* axis and the *j* axis foreshadows the inhomogeneous solid-like features at lower temperatures.

A correlation length can be similarly defined from the site of the perturbation. Again, a mean-field square-root divergence with proximity to the critical temperature is obtained. In comparison to the fully dense case, however, at the same relative distance to the critical point, the correlation length is significantly longer here.

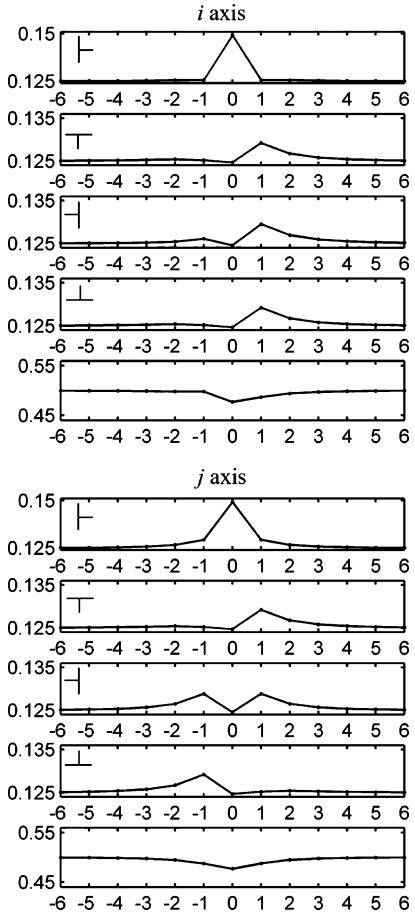

Figure 6. The probability of being in each state as a function of position along the *i* and *j* axes, after a small pinning force with magnitude 0.01β favoring state 1 is applied at site (0,0) to a solution. The unperturbed solution-like state $\beta\epsilon = 1.7$, $\rho = 0.5$ has an equal probability (0.125) of being in each rotational state of the solute and a 0.5 probability of being solute (state 5).

5.5. DMF Simulations: Gelation as a Result of Arrested Phase Separation. In the two phase region, a wide range of structures is observed. The results of a stepwise quench in which the lattice is equilibrated at successively lower temperatures show very different characteristics than those of a lattice that is quenched to the same conditions in one step. To illustrate this effect, we first present the results of a quench of the system that is equal parts T-shaped molecules and solvent.

When the simulation is taken from the "high"-temperature solution phase to just below the liquid/liquid coexistence curve, it phase-separates without any (orientational) ordering. Both the solute-rich phase and the solvent-rich phase retain liquid character. If we further quench this structure to below many spinodals, but at a temperature such that the solute-rich phase is above the triple point, we observe the formation of a layer of oriented molecules at the interface (Figure 7a). This film occurs at all of the solute-rich phase boundaries. The bulk of the molecule-rich phase retains the expected liquid-like character. Small droplets of solvent-rich phase have developed within the initial solute-rich droplet. If this system is cooled further so that the solute-rich phase is below the triple point, then the solute-rich phase solidifies into a glass-like structure (Figure 7b). The presence of small, solvent-rich voids within the glassy droplet suggests a very dense gel-like structure.

If we plunge the system with equal parts molecules and solvent below many spinodals and near or below the triple point, we observe networked gel-like structures. Figure 8a presents a

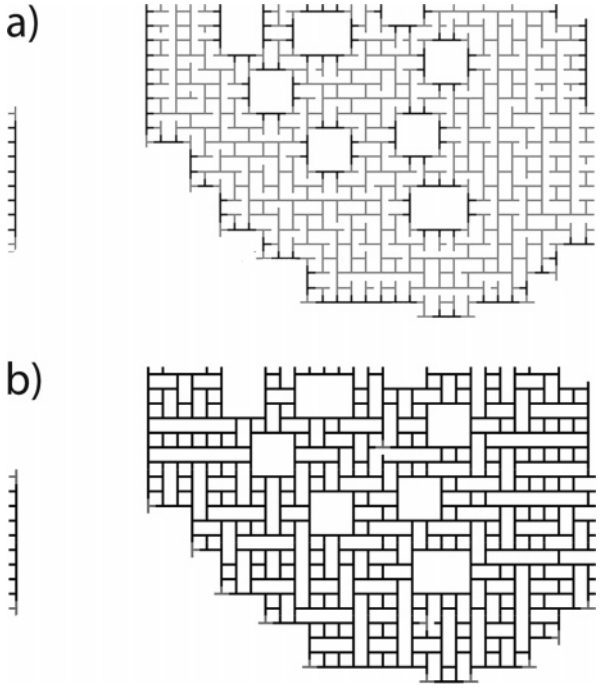

Figure 7. DMF simulation results at $\rho = 0.5$: (a) A phase-separated droplet shows the self-surfactant character of the molecules. A simulation in the solution state was initially instantaneously quenched to $\beta\epsilon = 2$ and allowed to equilibrate before instantaneously quenching to a final temperature of $\beta\epsilon = 3$. (b) A glassy droplet was successively equilibrated from a solution to $\beta\epsilon = 2$, $\beta\epsilon = 3$, and then, as shown, at $\beta\epsilon = 4$. Sites shown in gray are not oriented but instead retain their liquid character.

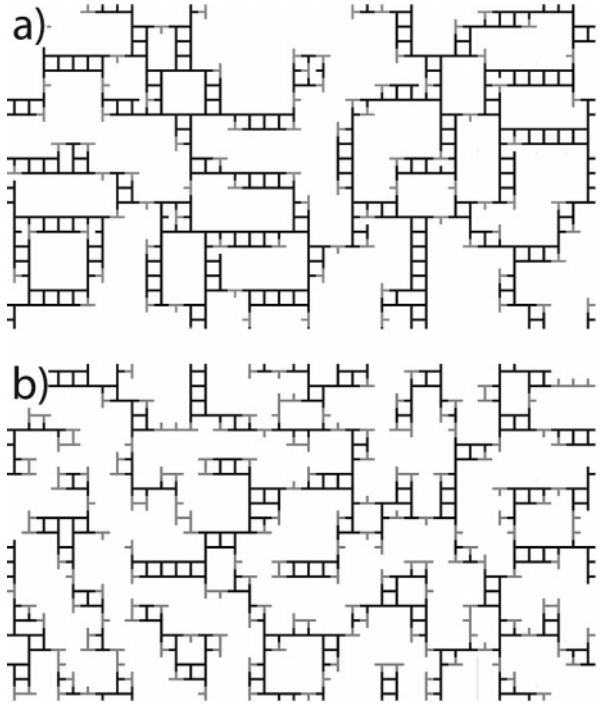

Figure 8. DMF simulation results at $\rho = 0.5$: (a) a gel that results from a simulation instantaneously quenched from a solution state to $\beta\epsilon = 4$, and (b) a gel quenched from a solution state to a lower temperature $\beta\epsilon = 10$. Sites in gray retain their liquid-like character.

dramatic example of the highly ramified structure that is the result of an instantaneous quench. The structure is very different from the more stepwise quenched structure in Figure 7b, despite resulting from simulations at the same final conditions. Experimentally, such differences in features are closely dependent on

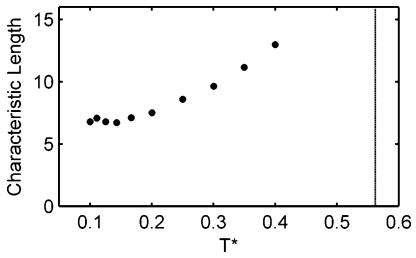

Figure 9. DMF simulation results at $\rho = 0.5$: the characteristic length (defined as 2π over the peak position of the circularly average structure factor) as a function of the quench depth given in dimensionless temperature, $T^* \equiv (\beta\epsilon)^{-1}$. The data are the result of averaging over 40 simulations of an 80×80 lattice. The vertical line indicates the critical temperature.

the "processing conditions".[51] Our model replicates a wide variety of morphologies by changing the quench conditions and volume fraction of molecules.

Overall, if we quench a simulation in very small increments from the solution phase, we allow for phase separation to proceed unhindered. However, at some temperature below the triple point, the phase separation transitions from liquid/liquid separation to liquid/solid separation. The solid phase is a disordered, glassy phase, and the simulation is structurally arrested. As the simulation is further cooled small voids of solvent-rich phase will accumulate within the molecule-rich phase. The resultant structure is a very dense gel. In a similar manner, if we quench from the solution phase directly to below the triple point, the phase separation is arrested by the onset of the solid phase. However, since there is not sufficient time for liquid/liquid phase separation before the onset of vitrification, the structure is much less dense and has a networked characteristic.

The length scale of the gel depends on the quench depth. We compare an instantaneous quench to a moderate temperature (Figure 8a) with a quench to a very low temperature (Figure 8b). Although the system is initially at the same identical liquid conditions, the deeper quench results in a smaller feature size. We can quantify the length scales of the gel by examining the peak position of the density−density structure factor.[52] As can be noted in Figure 9, there is a clear trend toward a smaller characteristic length with temperature. This is consistent with our analysis of the cascade of spinodals in section 5.3; the instability with respect to spatial inhomogeneity shifts to smaller length scales as temperature decreases.

More precisely, however, the observed dependence on the temperature is a consequence of both thermodynamic and kinetic factors. It is well-known that in spinodal decomposition, the most unstable mode has a wavelength inversely proportional to the square root of the distance to the critical temperature.[53] In a simple binary mixture, coarsening occurs beyond this initial growth of the most unstable mode. However, in our system, once the concentration of the T-molecule-rich phase becomes sufficiently high, vitrification sets in, which arrests any further domain growth. The deeper the temperature quench, the smaller the length scale of the initial instability and, hence, the smaller the length scale at which the system gets arrested. The decrease in length scale with deeper quench was observed in a colloidal gel system studied by Dinsmore and Weitz.[5]

We note that there is an interesting transition between coarsening to macroscopically phase-separated states at temperatures just below the critical point and developing ramified microstructures at lower temperatures (still above the triple point). We speculate that this transition reflects the tendency toward inhomogeneous structures at finite length scales associated with the lower spinodals, which are more of microphase separation than of macrophase separation in nature.

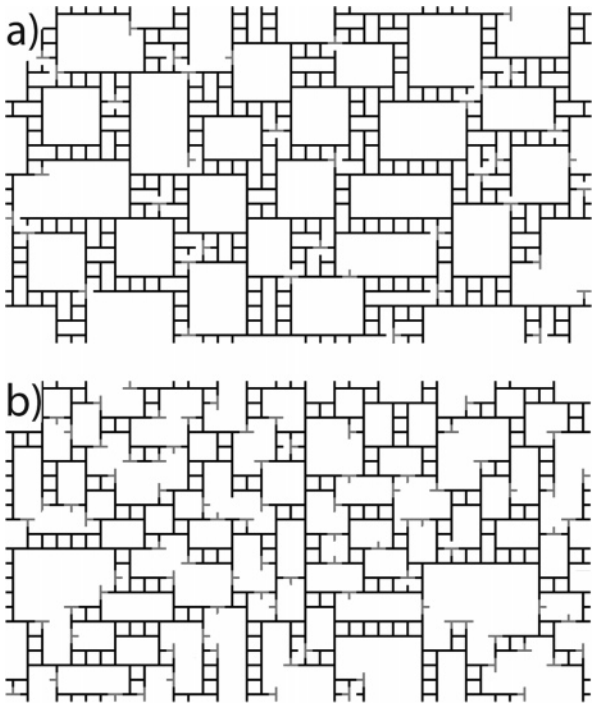

Figure 10. DMF simulation results $\rho = 0.65$: (a) a two-step quench starting with the solution phase instantaneously quenched to $\beta\epsilon = 3$ and allowed to equilibrate before being quenched to $\beta\epsilon = 5$, and (b) a single-step quench from the solution state directly to $\beta\epsilon = 5$. Sites shown in gray are not oriented but instead retain their liquid character.

Simulations at similar temperatures but higher volume fraction of molecules demonstrate other features of the gel-like structures that can be formed. At these higher concentrations, we can form dense gels that span the space of the simulation. Figure 10a is a result of a two-step quench. While the solvent-rich voids are of the same scale as the glassy droplet in Figure 7b, this structure more resembles a foam. As before, when the simulation is quenched directly, it results in a more networked structure with smaller mesh sizes (Figure 10b).

Exploring the portion of the two-phase region at a low volume fraction of the T-shaped molecules, we observe the formation of suspended small droplets and fibrils. Given enough time to first phase-separate under liquid/liquid conditions before quenching below the triple point, small droplets of glass form. On the other hand, if quenched quickly, ladder-like fibrils result. These suspended structures could be due to the lack of a cluster diffusion mechanism in our dynamics; it is not clear, however, when such a mechanism is included, whether these droplets and fibrils will aggregate or coalesce. As the surfaces of these structures have relatively few unbonded association sites, even if the droplets or fibrils were to come into contact they might not aggregate. For the suspended structures to aggregate or coalesce, internal restructuring is required, which is greatly inhibited by the vitrification of the solute below the triple point.[54] Therefore, since these structures still correspond to local free-energy minima, we include them in the class of gel structures in our consideration, even though they lack the connectivity of a space-spanning network usually associated with gels.

It has long been noted that gel formation in the two-phase region is highly dependent on the conditions of formation, much to the chagrin of experimentalists. De Gennes observed that incomplete phase separation due to an effective change in solvent quality during polymer association and slow kinetics

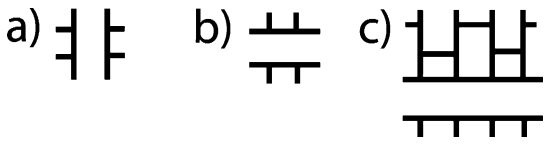

Figure 11. Determining the number of ground states: (a,b) two basic building blocks from which we can demonstrate that there is an exponential number of ground-state configurations, and (c) an additional state not accounted for in the previous estimation.

of solvent diffusion lead to heterogeneous gels.[55] Our model also results in heterogeneous gels; however, in our case, the inhibition of phase separation is due to kinetic arrest arising from the formation of a glassy state in the solute-rich regions.

We develop a picture of the phase behavior of these systems being arrested in a metastable state by the onset of a glass-like structure. This incomplete phase separation, though driven by the thermodynamic conditions, represents a kinetic phenomenon. The features that we observe are determined by the confluence of the thermodynamic and kinetic conditions.

6. Structural Relaxation in the Glassy State

Thus far, we have been focusing on the thermodynamic and structural properties of our system. The diversity in morphologies observed in the gelation regime highlights the critical role of kinetics as well. In this section, we study the structural relaxation in the fully dense phase. Our discussion has been focused on the mean-field phase diagram and structures obtained with DMF simulations. Within this framework, once the system finds itself in a local free-energy minimum, no relaxation is possible from this state. However, it is possible to study the relaxation in the liquid state as the system is cooled. We explore the relaxation of the system in the fully dense case by examining the energy landscape features and the relaxation mechanism at low temperatures. We also include results from both DMF and MC simulations that show dynamics characteristic of glass-forming systems.

6.1. Features of the Energy Landscape. The energy landscape paradigm has become an important guide to consider the thermodynamic signatures of glass-like systems (for reviews, see refs 30 and 56−58). An unusual feature of our model is the exponentially large number of states in which all the associating sites are satisfied. The lamellar crystalline state is but one of these states (Figure 3a). A lower bound on the number of ground states in the fully dense case can be estimated by the following argument. We note that a foursome of molecules can be organized in two energetically equivalent ways that present to the neighbors of this grouping the same number of associating sites (Figure 11a,b). A fully satisfied lattice can be created by using this foursome as the repeating units in either of these two states. Thus, on a lattice of size n there are $2^{n/4}$ satisfied configurations. This is a lower bound, as more complex repeating units can be used to generate the lattice (Figure 11c), and there can also be structures that cannot be created using any repeating units.

As the temperature in a glass-forming liquid nears the glass transition T_g, it has been empirically noted that the stretched exponential functional form, $\theta(t) = \exp[-(t/\tau)^\beta]$, fits both experimental and simulation measurements of the structural relaxation well. The dramatic increase of relaxation time upon cooling in fragile glasses can be described well by the Vogel−Fulchur (VF) equation, $\tau/\tau_o = \exp[D/(T - T_o)]$, with the value of D being the "fragility index".[59]

The large degeneracy of the minima in the free-energy landscape, together with the relatively low barriers separating

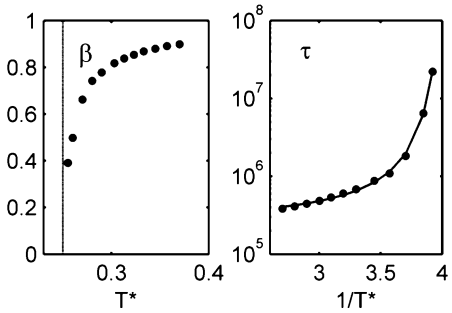

Figure 12. Glassy dynamics shown in DMF simulations: a stretched exponential functional form is fit to the relaxation of the order parameter (eq 15). The figures show the temperature dependence of the stretching exponent β and characteristic time τ. The vertical line indicates the mean-field transition temperature.

the minima (in the sense that the rearrangements can be made by breaking a small number of bonds) implies fragile-liquid behavior. However, at sufficiently low temperatures, the relaxation mechanism involves creating isolated unpaired bonds, with a well-defined energy scale (see section 6.4 for more discussion). This suggests an Arrhenius dependence of the relaxation on temperature, which is associated with strong-liquid behavior. Therefore we expect that our systems will exhibit fragile-liquid characteristics at higher temperatures and strong-liquid characteristics at very low temperatures.

6.2. Relaxation in DMF Simulations. The DMF simulation technique described in section 3 is employed for temperatures above the spinodal to observe the relaxation of small and random perturbations back to a uniform liquid state. To quantify the relaxation behavior, we define an order parameter:

$$m(t - t_0) = \frac{\sum_{i=1}^{N}\sum_{a=1}^{4}\sqrt{(p_a(i;t) - 0.25)^2}}{\sum_{i=1}^{N}\sum_{a=1}^{4}\sqrt{(p_a(i;t_0) - 0.25)^2}} \qquad (15)$$

The decay of this function is found to be well fit by a stretched exponential form $m(t - t_o) = \exp\{-[(t - t_o)/\tau]^\beta\}$. Figure 12 shows the behavior of the exponent β and characteristic time τ as a function of temperature.

We find that, as the temperature decreases, β decreases significantly from 1, as is characteristic of a fragile liquid.[60] At the same time, the dependence of the relaxation time on temperature is well fit, described by the VF equation. Remarkably, the least-squares fit to the data in Figure 12 results in $T_o \cong 0.24$, very close to the theoretically predicted mean-field spinodal, implying an "ideal" glass transition at this temperature.[61] To see if this observed relaxation could be more a reflection of a critical slowing down rather than glassy dynamics, we have also fitted the relaxation time τ into $\tau = \tau_o|T/T_C - 1|^{-2\upsilon z}$, where υ and z are respectively the correlation length and dynamic scaling exponents; the mean-field values $\upsilon = 1/2$ and $z = 2$ are used.[62] We find that the fit is quite poor (not shown).

6.3. Relaxation in MC Simulations. To investigate relaxation without the restriction of the mean-field approximation, MC simulations are performed. The rules of motion are described in section 2. Simulations are equilibrated at each temperature over many MC steps (each step is defined as one randomly proposed move in configuration space that may or may not be performed).[63] We then perform 1.6×10^6 MC steps on the initial configuration and track the correlation function $\theta(t - t_0)$, defined as the fraction of sites on a lattice that have not undergone any

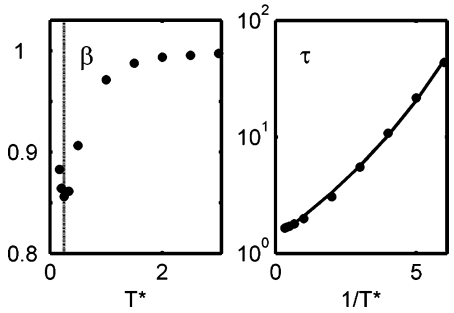

Figure 13. Glassy dynamics shown in MC simulations: a stretched exponential functional form was fit to the averaged relaxation of the correlation function. The figure shows the values of the stretching exponent β and the characteristic time τ. The vertical line indicates the mean-field transition temperature.

transition to other states from time t up to t_0. We repeat this procedure 10 times and average the resulting correlation functions. We then fit $\theta(t - t_0)$ with a stretched exponential form and repeated the process. The temperature dependence of β and τ are shown in Figure 13. Note the small increase in β at the lowest temperatures; this may reflect the approach to the strong-liquid limit (this will be discussed further in section 6.4). Our results are similar to that of a simulation for liquid silica, which found that the material behaved thermodynamically as a "fragile" liquid at high temperature, while behaving as a "strong" liquid at low temperatures.[64]

When the VF equation is fit to the relaxation time as a function of temperature, we find $T_o \cong 0.07$ which is well below the mean-field spinodal temperature. This is a consequence of activated events allowing for exploration of the energy landscape below the onset of inhomogeneous energy minima. As in experiments, the glass transition is a kinetic phenomenon defined by the relaxation time of the system. As equilibration at very cold temperatures takes an exceedingly long time, and since our main focus in this present work is illustrating some structural and thermodynamic properties, we have not yet evaluated temperatures as low as T_o found from the VF fit; these calculations will be preformed in the future.

Overall, this MC simulation shows dynamics that reflect a "stronger" liquid than that observed with DMF simulations. Various explanations of deviations of T_o from T_k, which are generally greater for "stronger" liquids than they are for more "fragile" liquids, have been proposed.[60,65] The fundamental reason appears to be decoupling of the thermodynamics (distribution of energy minima) and kinetics (details of the depth of the well around the minima) on the landscape.[66] Thus, it is not surprising that the MC simulations, which reflect both thermodynamics and kinetics, would reveal different results than those of the DMF simulations, which involve the thermodynamics alone.

6.4. Relaxation Mechanism at Low Temperatures. The landscape features of our model imply a different relaxation mechanism than that commonly associated with structural relaxation in supercooled liquid as it approaches the glass transition, which usually involves hopping between deep free-energy minima separated by large, energetic barriers.[57,61,67,68] In our model, proceeding from one ground state to another involves only a small energy penalty. All that is required is for one molecule to rotate, breaking a pair of bonds. This pair of unsatisfied T-shaped molecules can then diffuse over the lattice, changing the state of the system at each time-step, until they annihilate themselves by finding another unpaired T-shaped molecule. We can directly observe this behavior in our MC simulations. At low temperatures, the concentration of such unpaired molecules is roughly $\exp(-\beta\epsilon)$. The area per unpaired molecule is thus $\exp(\beta\epsilon)$. Assuming this molecule diffuses freely with a diffusivity ω, the area visited in time t is proportional to the mean-square distance traveled by the molecule, $R^2 \sim \omega t$. The system will have relaxed from its initial configuration if an unpaired molecule has visited an area of the size of the area per unpaired molecule. Thus, the relaxation time is simply $\tau \sim \omega^{-1} \exp(\beta\epsilon)$.[69] While this argument does not predict the time dependence of the relaxation dynamics, it shows that the slowing down of the dynamics as temperature decreases is due to the decrease in the number of (essentially isolated) "mobile" (i.e., unpaired) molecules. This is a very different process than that of an activated process on a landscape with deep energy minima, which often requires concerted or facilitated motion. Instead of the glass or gel being the result of high-energy barriers, in our model, they result from the multiplicity of energetically degenerate states.

The temperature dependence predicted from the low-temperature argument is Arrhenius. Thus, at very low temperatures, our model should behave like a strong liquid; this is consistent with the upward turn of the stretching exponent β as temperature is decreased at very low values and the observation that the right-most data for the characteristic time τ on the semilog plot (Figure 13) appears to approach a straight line.

7. Conclusions

The strength of this lattice model lies in its simplicity and its ability to capture a wide range of morphological behavior without imposing an artificial constraint that causes the system to be frustrated. In our model, amorphous vitrified (glass or gel-like) structures arise, not because of frustration, but because of the ready availability of a large number of inhomogeneous free-energy minima; this observation is consistent with the recent thermodynamic picture of structural glasses resulting from self-generated randomness as a result of a large number of degenerate ground states.[70−73] Although nontrivial, glassy dynamics do not require the existence of a large number of inhomogeneous free-energy minima; however, the existence of such minima necessitates a change in the dynamics. Shifting from liquid-like to glass-like, the relaxation of the system now requires leaving the free-energy minima through thermal activation. In the DMF simulations, which do not allow for thermal fluctuations, the dynamic transition temperature occurs at the mean-field spinodal. When activated motion is possible in the MC simulations, the dynamic transition temperature is lower than the spinodal. However, it is important to note that both simulations exhibit glassy behavior at low temperatures.

An important result of this work concerns the nature of the gel phase and its relationship to the glass phase. Various authors have noted the similarities between these two classes of materials.[9,74−76] Our model allows us to explore this relationship. From the structural and thermodynamic point of view, both states of matter result from the proliferation of a large number of inhomogeneous free-energy minima, which are ultimately connected to the underlying mean-field spinodals with respect to inhomogeneous structural fluctuation. In our model, the glassy state is obtained as a result of the quenching of the liquid phase in the high density, one-phase region of the phase diagram below the temperature for the appearance of an exponentially large number of inhomogeneous free-energy minima. The gel state can be viewed as an extension of the glassy state into the two-phase region or, equivalently, as an incomplete phase separation arrested by the onset of glass transition. The length scale of the gel phase is determined primarily by the most unstable, that is,

fastest-growing, mode—a deeper quench leads to a network with smaller mesh size. The arrest of phase separation is a result of the system having reached a state of local free-energy minimum. At such free-energy minima, the deterministic thermodynamic driving force vanishes; further evolution of the structure must require overcoming free-energy barriers. Such a relaxation mode is very different from the coarsening process in a typical phase-separating binary fluid; in our case, the relaxation of this structurally arrested state is more properly described as an aging process.

The behaviors exhibited by our model relate well to those of colloidal gels in particular. Colloidal gels are akin to a solvated glass that has short-range attractive interactions,[9,76] a feature that we capture in our model. The decrease in the characteristic length scale with quench depth lends further credence to this correlation. While it might be surprising that this is the case, given the isotropic nature of a colloidal particle, we believe that this suggests that the steric constraints on the system are fundamentally similar to an anisotropic interaction in a lattice model. Indeed, a two-dimensional square lattice model in which each site can only form up to three attractive interactions with its nearest neighbors is identical to our T-shaped molecule model.

Our model can be extended in several directions. First, as alluded to in the model description, it is straightforward to add an isotropic term that either favors or disfavors nearest neighbor contacts between the solute molecules. The latter type would suppress the critical temperature, possibly making it lower than the glass transition in the fully dense case. The resulting phase diagram would appear closer to the phase diagram for colloidal particles with short-ranged attractions.[9] Second, it is possible to construct three-dimensional versions of the model. Besides the obvious fact that most systems are in three dimensions, the mean-field approximations are more accurate in three dimensions than in two. Finally, exploring the dynamics of the solvated state should prove interesting and help investigate the gelation transition as it relates to vitrification. We plan to pursue these directions in the future.

Acknowledgment. This research was supported in part by the National Science Foundation through the Center for the Science and Engineering of Materials.

References and Notes

(1) Bergenholtz, J.; Fuchs, M.; Voigtmann, T. *J. Phys.: Condens. Matter* **2000**, *12*, 6575.

(2) Zaccarelli, E.; Foffi, G.; Dawson, K. A.; Buldyrev, S. V.; Sciortino, F.; Tartaglia, P. *J. Phys.: Condens. Matter* **2003**, *15*, S367.

(3) Sciortino, F.; Mossa, S.; Zaccarelli, E.; Tartaglia, P. *Phys. Rev. Lett.* **2004**, *93*, article no. 055701.

(4) Pham, K. N.; Puertas, A. M.; Bergenholtz, J.; Egelhaaf, S. U.; Moussaid, A.; Pusey, P. N.; Schofield, A. B.; Cates, M. E.; Fuchs, M.; Poon, W. C. K. *Science* **2002**, *296*, 104.

(5) Dinsmore, A. D.; Weitz, D. A. *J. Phys.: Condens. Matter* **2002**, *14*, 7581.

(6) Ren, S. Z.; Sorensen, C. M. *Phys. Rev. Lett.* **1993**, *70*, 1727.

(7) Ikkai, F.; Shibayama, M. *Phys. Rev. Lett.* **1999**, *82*, 4946.

(8) Gang, H. D.; Krall, A. H.; Cummins, H. Z.; Weitz, D. A. *Phys. Rev. E* **1999**, *59*, 715.

(9) Foffi, G.; De Michele, C.; Sciortino, F.; Tartaglia, P. *Phys. Rev. Lett.* **2005**, *94*, article no. 078301.

(10) Del Gado, E.; Fierro, A.; de Arcangelis, L.; Coniglio, A. *Phys. Rev. E* **2004**, *69*, article no. 051103.

(11) Kauzmann, W. *Chem. Rev.* **1948**, *43*, 219.

(12) Granasy, L.; Pusztai, T.; Borzsonyi, T.; Warren, J. A.; Douglas, J. F. *Nat. Mater.* **2004**, *3*, 645.

(13) Bryngelson, J. D.; Wolynes, P. G. *J. Phys. Chem.* **1989**, *93*, 6902.

(14) Silbert, L. E.; Ertas, D.; Grest, G. S.; Halsey, T. C.; Levine, D. *Phys. Rev. E* **2002**, *65*, article no. 051307.

(15) Mezard, M.; Parisi, G.; Virasoro, M. A. *Spin Glass Theory and Beyond*; World Scientific: Singapore, 1987.

(16) Palmer, R. G.; Stein, D. L.; Abrahams, E.; Anderson, P. W. *Phys. Rev. Lett.* **1984**, *53*, 958.

(17) Fredrickson, G. H.; Andersen, H. C. *J. Chem. Phys.* **1985**, *83*, 5822.

(18) Jackle, J.; Eisinger, S. *Z. Phys. B: Condens. Matter* **1991**, *84*, 115.

(19) Weber, T. A.; Fredrickson, G. H.; Stillinger, F. H. *Phys. Rev. B* **1986**, *34*, 7641.

(20) Garrahan, J. P.; Chandler, D. *Proc. Natl. Acad. Sci. U.S.A.* **2003**, *100*, 9710.

(21) Aranovich, G. L.; Donohue, M. D. *J. Chem. Phys.* **2002**, *116*, 7255.

(22) Biroli, G.; Mezard, M. *Phys. Rev. Lett.* **2002**, *88*, article no. 025501.

(23) Cellai, D.; Cuevas, H.; Lawlor, A.; McCullagh, G. D.; Dawson, K. A. *Phys. Rev. E* **2004**, *70*, article no. 022401.

(24) Ben-Naim, A. J. *J. Chem. Phys.* **1971**, *54*, 3682.

(25) Bell, G. M.; Lavis, D. A. *J. Phys. A* **1970**, *3*, 568.

(26) Silverstein, K. A. T.; Haymet, A. D. J.; Dill, K. A. *J. Am. Chem. Soc.* **1998**, *120*, 3166.

(27) Girardi, M.; Figueiredo, W. *J. Chem. Phys.* **2004**, *120*, 5285.

(28) Poole, P. H.; Sciortino, F.; Grande, T.; Stanley, H. E.; Angell, C. A. *Phys. Rev. Lett.* **1995**, *73*, 1632.

(29) Dellavalle, R. G.; Andersen, H. C. *J. Chem. Phys.* **1992**, *97*, 2682.

(30) Debenedetti, P. G. *Metastable Liquids: Concepts and Principles*; Princeton University Press: Princeton, NJ, 1996.

(31) Stillinger, F. H.; Debenedetti, P. G. *J. Phys. Chem. B* **2005**, *109*, 6604.

(32) Kumar, S. K.; Douglas, J. F. *Phys. Rev. Lett.* **2001**, *8718*, article no. 188301.

(33) Grant, M. C.; Russel, W. B. *Phys. Rev. E* **1993**, *47*, 2606.

(34) Kumar, S. K.; Panagiotopoulos, A. Z. *Phys. Rev. Lett.* **1999**, *82*, 5060.

(35) Shibayama, M.; Ikkai, F.; Moriwaki, R.; Nomura, S. **1994**, *27*, 1738.

(36) Singh, Y. *Phys. Rev. Lett.* **1985**, *54*, 1059.

(37) Kawasaki, K. In *Phase Transitions and Critical Phenomena*; Domb, C., Lebowitz, J. L., Eds.; Academic Press: London, New York, 1972.

(38) Landau, D. P.; Binder, K. *A Guide to Monte Carlo Simulations in Statistical Physics*; Cambridge University Press: New York, 2000.

(39) Wang, Z.-G. *Phys. Rev. A* **1992**, *45*, 692.

(40) Barker, A. A. *Aust. J. Phys.* **1965**, *18*, 119.

(41) Marconi, U. M. B.; Tarazona, P. *J. Chem. Phys.* **1999**, *110*, 8032.

(42) Fraaije, J. G. E. M. *J. Chem. Phys.* **1993**, *99*, 9202.

(43) It is not apparent that, in the crystal-like state, the probabilities of the three nonpreferred orientations should be equal as there is not a symmetry-breaking event in the direction transverse to the lamella direction. However, our calculations found that this assumption holds for all temperatures.

(44) Klein, W. *Phys. Rev. Lett.* **2000**, *85*, 1270.

(45) Bagchi, B.; Cerjan, C.; Rice, S. A. *J. Chem. Phys.* **1983**, *79*, 5595.

(46) Woodcock, L. V. *Ann. N. Y. Acad. Sci.* **1981**, *371*, 274.

(47) Zhang, C.-Z.; Wang, Z.-G. *Phys. Rev. E.* **2006**, article no. 064601.

(48) Reichl, L. E. *A Modern Course in Statistical Mechanics*, 2nd ed.; John Wiley & Sons: New York, 1998.

(49) The coefficient 9/8 in the energy term arises from multiplying the probability that two arms of molecules on adjacent sites are touching, multiplied by one-half of the coordination number (3/4*3/4*4/2).

(50) Rubinstein, M.; Dobrynin, A. V. *Curr. Opin. Colloid Interface Sci.* **1999**, *4*, 83.

(51) Guenet, J.-M. *Thermoreversible Gelation of Polymers and Biopolymers*; Academic Press: London, San Diego, CA, 1992.

(52) Press: W. H.; Teukolsky, S. A.; Vertterling, W. T.; Flannery, B. P. 13.8 Spectral Analysis of Unevenly Sampled Data. In *Numerical Recipes in Fortran 77: The Art of Scientific Computing*, 2nd ed.; Cambridge University Press: New York, 2001; Vol. 1, p 569.

(53) Cahn, J. W. *Acta Metall.* **1961**, *9*, 795.

(54) Stable glassy colloidal clusters that appear not to aggregate or coalescence have been observed experimentally; Weitz, D. A. Harvard University, Cambridge, MA. Private communication, 2005.

(55) De Gennes, P.-G. *Scaling Concepts in Polymer Physics*; Cornell University Press: Ithaca, NY, 1979.

(56) Angell, C. A.; Ngai, K. L.; McKenna, G. B.; McMillan, P. F.; Martin, S. W. *J. Appl. Phys.* **2000**, *88*, 3113.

(57) Debenedetti, P. G., Truskett, T. M., Lewis C. P. Theory of Supercooled Liquids and Glasses. In *Advances in Chemical Engineering; 28. Molecular Modeling and Theory in Chemical Engineering*; Chakraborty, A., Ed.; Academic Press: San Diego, CA, 2001.

(58) Sciortino, F. *J. Stat. Mech.* **2005**, article no. p05015.

(59) Angell, C. A. *J. Non-Cryst. Solids* **1988**, *102*, 205.

(60) Xia, X. Y.; Wolynes, P. G. *Phys. Rev. Lett.* **2001**, *86*, 5526.

(61) Adam, G.; Gibbs, J. H. *J. Chem. Phys.* **1965**, *43*, 139.

(62) Onuki, A. *Phase Transition Dynamics*; Cambridge University Press: Cambridge, 2002.

(63) To reach cooler temperatures, we started with a high-temperature simulation, which reaches equilibrium relatively quickly. This was then used

as the starting point for the next coolest temperature. Working in this stepwise fashion, colder and colder temperatures were reached.

(64) Saika-Voivod, I.; Poole, P. H.; Sciortino, F. **2001**, *412*, 514.

(65) Tanaka, F. *Macromolecules*, **2003**, *36*, 5392.

(66) Stillinger, F. H.; Debenedetti, P. G. *J. Chem. Phys.* **2002**, *116*, 3353.

(67) Stillinger, F. H.; Weber, T. A. *Phys. Rev. A* **1982**, *25*, 978.

(68) Stillinger, F. H.; Weber, T. A. *Science* **1984**, *225*, 983.

(69) This argument is based on the exchange dynamics for the lattice. However, the flip (rotation) dynamics (as employed here in the DMF) would yield the same result. With a concentration of unpaired molecules of $\exp(-\beta\epsilon)$, the probability that a randomly chosen satisfied molecule is turned into an unpaired one in unit time is simply $\omega \exp(-\beta\epsilon)$. The time it takes for the lattice to relax is such that $\tau\omega \exp(-\beta\epsilon) \sim 1$, or $\tau \sim \omega^{-1} \exp(\beta\epsilon)$.

(70) Monasson, R. *Phys. Rev. Lett.* **1995**, *75*, 2847.

(71) Nussinov, Z.; Rudnick, J.; Kivelson, S. A.; Chayes, L. N. *Phys. Rev. Lett.* **1999**, *83*, 472.

(72) Mezard, M.; Parisi, G. *J. Phys.: Condens. Matter* **2000**, *12*, 6655.

(73) Schmalian, J.; Wolynes, P. G. *Phys. Rev. Lett.* **2000**, *85*, 836.

(74) Puertas, A. M.; Fuchs, M.; Cates, M. E. *Phys. Rev. Lett.* **2002**, *88*, article no. 098301.

(75) Dawson, K. A. *Curr. Opin. Colloid Interface Sci.* **2002**, *7*, 218.

(76) Sciortino, F. *Nat. Mater.* **2002**, *1*, 145.